J Mater Sci (2011) 46:4314–4317
DOI 10.1007/s10853-011-5299-9

IIB 2010

Thermal stability of Al/nanocrystalline-Si bilayers investigated by in situ heating energy-filtered transmission electron microscopy

Z. M. Wang · L. Gu · L. P. H. Jeurgens · E. J. Mittemeijer

Received: 30 August 2010 / Accepted: 17 January 2011 / Published online: 5 February 2011
© Springer Science+Business Media, LLC 2011

Abstract In situ heating energy-filtered transmission electron microscopy was employed to investigate the interfacial intermixing/reactions during thermal annealing of Al/nanocrystalline-Si (nc-Si) bilayers in the temperature range of 150–500 °C. In comparison with the Al/amorphous-Si (a-Si) bilayer, the Al/nc-Si bilayers were found to be much more stable against thermal annealing. Wetting and c-Si growth processes along Al grain boundaries, which take place during annealing of Al/a-Si bilayers, do not occur in Al/nc-Si bilayers, because of the lack of thermodynamic driving forces in the latter case. As a consequence, also in contrast with Al/a-Si bilayers, no layer exchange occurs in Al/nc-Si bilayers, not even after annealing at 500 °C. Instead, intermixing of Al/nc-Si is realized at the Al/nc-Si interface by the formation of Al spikes growing into the nc-Si sublayers at temperatures higher than 300 °C. The relatively low Al-spike formation temperature in Al/nc-Si systems, as compared with that for Al/single-crystalline Si systems, is ascribed to the higher Gibbs energy of nanocrystalline Si as compared to single-crystalline Si.

Introduction

Thin films of amorphous and nanocrystalline silicon are key materials in thin-film solar cells [1, 2] and flat-panel displays [3]. In such thin-film devices, contacts between amorphous/nanocrystalline silicon with metal electrodes commonly exist. Since a modest/high temperature annealing process is often required to stabilize the device performance, the thermal stability of the metal/silicon contacts has become an important concern in device fabrications.

It is well known that the contact between amorphous silicon (a-Si) and a metal is thermally unstable [4]. When put into contact with a metal, a-Si starts to crystallize at much lower temperatures than its bulk crystallization temperature; a phenomenon commonly referred to as metal-induced crystallization (MIC). During a MIC process, substantial intermixing and/or reaction of the silicon and metal layers usually occur. As an example, a-Si in a-Si/Al bilayers crystallizes at a temperature as low as 150 °C [5] and the crystallization of a-Si is associated with intermixing of the Si and Al sublayers, even leading to a complete layer exchange of Si and Al upon full crystallization of the a-Si sublayer at a low temperature of 250 °C [6]. Direct contact of a-Si and Al (or other metal electrodes) should therefore be avoided in thin-film a-Si devices.

Nanocrystalline silicon (nc-Si) may offer better electrical and structural performances than a-Si in flat-panel displays and photovoltaic devices, and has therefore attracted huge interest in recent years [1–3]. However, the thermal stability of nc-Si/metal contacts has not been investigated in detail, as compared with the a-Si/metal [4] and single-crystalline-Si/metal contacts [7, 8]. In this study, in situ heating energy-filtered transmission electron microscopy (EFTEM) was employed to investigate the interaction of Al and nanocrystalline silicon during thermal annealing at different temperatures. The in situ heating EFTEM technique is essential in this project because it provides a unique tool to monitor the reactions at well-defined (fixed) locations in the bilayer microstructure,

Z. M. Wang (✉) · L. Gu · L. P. H. Jeurgens · E. J. Mittemeijer
Max Planck Institute for Metals Research, Heisenbergstr. 3, 70569 Stuttgart, Germany
e-mail: z.wang@mf.mpg.de

E. J. Mittemeijer
Institute for Materials Science, University of Stuttgart, Heisenbergstr. 3, 70569 Stuttgart, Germany

which is not possible by an ex situ approach. It is found that the thermal stability of nc-Si/Al contacts is much higher than that of a-Si/Al contacts, and is close to that of single-crystalline-Si/Al contacts.

Experimental

Al/nc-Si bilayer specimens were prepared in a customized, multi-chamber molecular beam epitaxy system (base pressure $< 2 \times 10^{-8}$ Pa). First, a 120-nm thick a-Si film was grown on a 50-nm SiO_2/Si(100) substrate at room temperature by thermal evaporation of pure Si (>99.999 wt%) from a Ta/W crucible using a high-temperature effusion cell. The a-Si film was then crystallized to nanocrystalline Si by in situ thermal annealing at 750 °C for 30 min. After cooling the specimen to room temperature, a 100-nm thick Al film was subsequently grown on top of the (now nanocrystalline) Si sublayer by thermal evaporation of pure Al (>99.999 wt%) from a Al_2O_3 crucible using a high-temperature effusion cell.

To prepare the cross-sectional TEM specimen, two pieces were cut from the Al/nc-Si bilayer specimen and bonded face-to-face (i.e. with the film sides in between) with epoxy glue. After mechanical thinning by grinding, the thin slice of material was embedded with the film surface parallel to the cylinder axis into a cylindrical polycrystalline Al_2O_3 tube of 3 mm diameter as a holder for the cross-sectional specimen. Then the tube was cut into slices. The slices underwent mechanical grinding, dimpling from both sides and finally ion thinning (Ar^+ ions with 4.0 keV energy and 1 mA ion current in a Fischione apparatus with liquid nitrogen cooling) for several hours to achieve electron transparency.

The in situ heating EFTEM experiments were performed in the Zeiss Sub-eV-Sub-Angstrom Microscope (SESAM, Carl Zeiss, Oberkochen, Germany), which is operated at 200 keV and equipped with an electrostatic monochromator and the MANDOLINE filter [9]. An energy resolution better than 100 meV is achieved routinely for electron energy-loss spectroscopy (EELS) analyses. The specimen was heated in situ using a Gatan 652 double-tilt heating stage in the SESAM microscope in the temperature range from 150 to 500 °C. Temperature of the holder tip was monitored by a calibrated silicon diode which provides a temperature response with a precision of 0.5 °C. At each temperature step, the specimen was isothermally annealed for 30 min, and then cooled to a stabilized temperature of 35 °C at which the EFTEM measurements were made. The EFTEM measurements were carried out as follows: First, a zero-loss bright-field TEM image was taken at the region of interest. Then an EFTEM series at energy losses from 12 to 20 eV in steps of 0.8 eV were acquired at the same region to form a 3D data cube. The total acquisition time for such an EFTEM series was less than 30 s, without any noticeable specimen drift occurring during the acquisition. The EELS spectrum (12–20 eV) at each pixel can thus be derived from the measured EFTEM series. A non-linear least squares Gaussian fitting of the EELS spectra was then applied to deduce the plasmon-loss energies accordingly in a pixel to pixel processing manner. In this way, maps of the plasmon peak position were generated, which can be correlated to the chemical distribution.

Results and discussion

A bright-field EFTEM micrograph of the cross section of the as-prepared Al/nc-Si bilayer is shown in Fig. 1a, at an energy loss (ΔE) of 16.5 eV. The 120-nm Si sublayer is confirmed to be nanocrystalline with an average (equiaxed) grain size of about 40 nm, whereas the 100-nm Al sublayer is polycrystalline with a columnar grain structure (average grain size $\sim$ 100 nm). The corresponding EFTEM mapping of the plasmon-loss peak energy of the as-prepared Al/nc-Si bilayer is also given in Fig. 1a (right-hand side). The bulk plasmon-loss energy of metallic Al is located at 15.0 eV, whereas that of nc-Si is located at 16.5 eV, in good agreement with literature values [10]. It also follows that the plasmon-loss energy is insensitive to microstructural features, such as grain orientations and boundaries. The plasmon loss energies at grain boundaries (GB) are observed to be similar to those at the interior of grains. This microstructural insensitivity of the technique allowed an independent, real-space observation of the intermixing process in Al/nc-Si during annealing. A narrow interfacial region ($\sim$2 nm), with plasmon-loss energy in between those of Al and Si, is observable between the Al and Si sublayers, which is ascribed to the interface roughness.

The Al/nc-Si bilayer was in situ heated in the SESAM microscope at temperatures from 150 to 500 °C. No apparent intermixing of Al and nc-Si occurred at temperatures below 300 °C. As shown in Fig. 1b, even after annealing at 300 °C for 30 min, the Al/nc-Si bilayer microstructure remained largely unchanged. However, small Al “spikes”, penetrating the nc-Si sublayer, had formed locally at the nc-Si sublayer adjacent to the Al/nc-Si interface, as evidenced by the decreased plasmon-loss peak energy at such locations (see arrow in the plasmon-loss energy mapping in Fig. 1b). Owing to the inevitable formation of passivating (native) oxide layers at the Al and Si surfaces of the TEM lamellae, the surface diffusion of Si along the oxidized Al and Si surfaces can be ruled out in the studied reaction temperature range. Thus, the observed Al spikes can only have formed within the nc-Si sublayer of the TEM lamellae and not at its surface. During

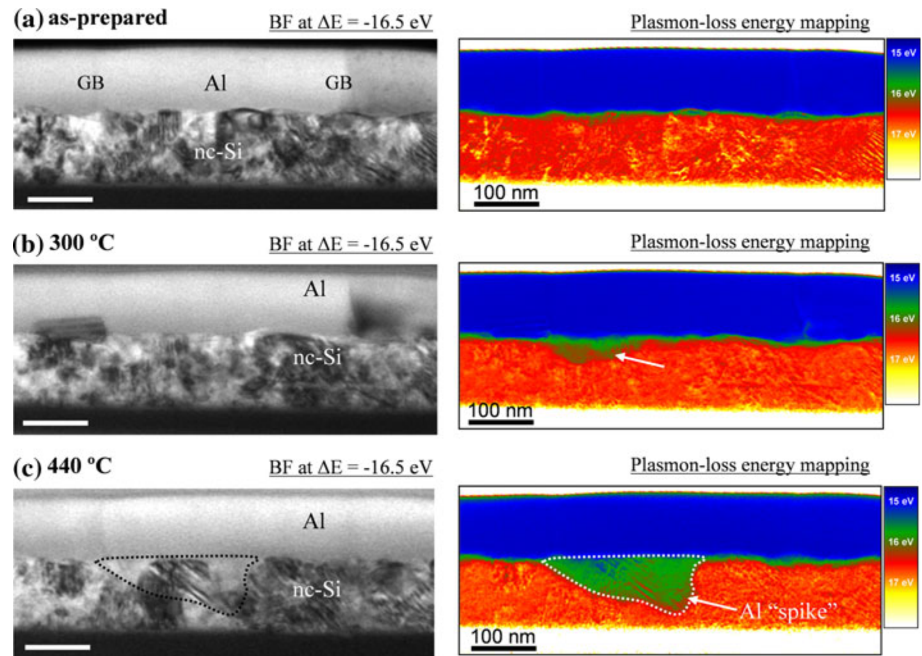

Fig. 1 In situ EFTEM observation, at the same location, of the interfacial reactions during annealing of the Al/nc-Si bilayer specimen: **a** as-prepared, **b** annealed at 300 °C for 30 min and **c** annealed at 440 °C for 30 min. The *left-hand side* figures are bright-field TEM images at the energy loss of 16.5 eV (which corresponds to the plasmon loss energy of Si), and the *right-hand side* figures are the corresponding mappings of the plasmon-loss peak energy (Al, Si)

annealing at higher temperatures, Al spikes were observed to grow at the expense of Si nanograins in the nc-Si sublayer; see Fig. 1c for the Al/nc-Si bilayer annealed at 440 °C.

The above described annealing behaviour of the Al/nc-Si bilayer is strikingly different from that observed for Al/a-Si bilayers. In the latter case, pronounced intermixing of Al and Si already occurs at very low temperatures of around 150 °C [11]. An additional EFTEM observation made in this study of the intermixing of Al and Si upon annealing of an Al/a-Si bilayer at a low temperature of 160 °C is shown in Fig. 2. Instead of the formation of Al spikes in the (in this case amorphous) Si sublayer, spikes of crystalline-Si develop at Al GBs in the Al sublayer.

Significant advances have been made in recent year towards fundamental understanding of the MIC of amorphous semiconductors [4, 12]. For Al-induced crystallization of a-Si in Al/a-Si bilayers, the process starts with wetting of high-angle Al GBs by a-Si at low temperatures (<200 °C), and continues by nucleation and growth of

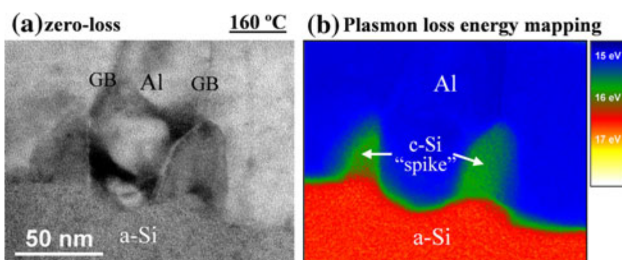

Fig. 2 EFTEM observation of an Al/amorphous-Si bilayer annealed up to 160 °C. **a** Zero-loss bright-field TEM image. **b** Mapping of plasmon-loss peak energy at the same location as (**a**)

crystalline Si at these wetted Al GBs [12]. Calculation of interface energies, following the methodology described in Ref. [13], revealed that there is indeed a thermodynamic driving force for wetting of high-angle Al GBs by *a-Si* [i.e. the Gibbs energy of a high-angle Al GB, γ_{AlGB} (0.34 J m^{-2} at 200 °C), is higher than two times the Gibbs energy of the Al/a-Si interface $2 \times \gamma_{\mathrm{Al|a\text{-}Si}}$ (0.14 J m^{-2} at 200 °C)] [12]. As a result of such MIC process, intermixing of Al and Si occurs already at very low temperatures in Al/a-Si bilayers, by initial wetting (by a-Si) and growth of c-Si along Al GBs at the location of the original Al sublayer, as observed in Fig. 2.

For the Al/nc-Si bilayer system, it follows from calculation of interface energies that the Gibbs energy of a high-angle Al GB, γ_{AlGB} (0.34 J m^{-2} at 200 °C), is smaller than two times the Gibbs energy of the Al/c-Si interface $2 \times \gamma_{\mathrm{Al|c\text{-}Si}}$ (0.90 J m^{-2} at 200 °C [12]). Therefore, high-angle Al GBs cannot be wetted by c-Si. Consequently, low-temperature intermixing (as discussed above for the Al/a-Si bilayer) cannot occur in the Al/nc-Si bilayer: the Al/nc-Si bilayer structure remained stable at annealing temperatures below 300 °C. In particular, at the high-angle Al GBs in the Al sublayer of the Al/nc-Si bilayer, as indicated in Fig. 1a, nothing happened during annealing (Fig. 1b, c). Note that $\gamma_{\mathrm{Al|c\text{-}Si}}$ consists of two terms: interfacial mismatch energy $\gamma^{\mathrm{mis}}_{\mathrm{Al|c\text{-}Si}}$ and interfacial chemical energy $\gamma^{\mathrm{chem}}_{\mathrm{Al|c\text{-}Si}}$ [12]. The latter term can be decreased upon dissolution of Si into the Al at relatively high temperatures (see below). However, since $\gamma^{\mathrm{mis}}_{\mathrm{Al|c\text{-}Si}}$ is much larger than $\gamma^{\mathrm{chem}}_{\mathrm{Al|c\text{-}Si}}$ (0.40 vs. 0.05 J m^{-2} at 200 °C [12]), any decrease in $\gamma^{\mathrm{chem}}_{\mathrm{Al|c\text{-}Si}}$ due to Si dissolution in Al would not result in a considerable decrease in $\gamma_{\mathrm{Al|c\text{-}Si}}$. Thus, wetting of

high-angle Al GBs by c-Si ($\gamma_{\mathrm{AlGB}} < \gamma_{\mathrm{Al|c\text{-}Si}}$) is also not thermodynamically favored after dissolution of Si in Al at elevated temperatures.

Upon increasing annealing temperature, of 300–500 °C, a small but measurable bulk solubility of Si in Al emerges (0.2–1.0 at.%), whereas the bulk solubility of Al in Si remains negligible [14]. Thus, certain dissolution of Si into Al grains can occur. This dissolution process can occur in a rather non-uniform manner: from both a thermodynamic and a kinetic point of view, it tends to start at locations where the smallest Si nanograins and/or highest defect densities occur [7]. Owing to such dissolution of Si (nanograins) in Al, voids form in the Si sublayers, which are subsequently filled by Al diffused from the Al sublayer. This explains the observed formation of Al spikes in the nc-Si sublayer upon annealing at temperatures above 300 °C (Fig. 1b, c). The formation of Al spikes in Si has also been observed upon annealing of Al/single-crystalline Si contact, but only at higher temperatures (above 400 °C) [7, 8]. It follows that the small Si nanograins, of relatively high Gibbs energy due to the relatively high ratio of grain-boundary area and bulk volume, are more easily dissolvable in Al. Comparing Fig. 1c (after Al spike formation) with Fig. 1a (before Al spike formation), the replacement of small Si nanograins by Al is clearly observable in the spike-forming region.

Conclusions

Al/nc-Si bilayers are much more stable than Al/a-Si bilayers upon thermal annealing. The wetting and c-Si growth processes along Al GBs, which occur in Al/a-Si bilayers at temperatures below 200 °C, cannot occur in Al/nc-Si bilayers at similar or even higher annealing temperatures: there is no thermodynamic driving force for such process. At temperatures higher than 300 °C, Al spikes, initiating at the Al/nc-Si interface, grow into the nc-Si sublayers, due to dissolution of Si in Al. The relatively low Al-spike formation temperature is ascribed to favored dissolution of Si nanograins of relatively high Gibbs energy as compared to single-crystalline Si, due to a high ratio of grain-boundary area and bulk volume and, possibly, a relatively high defect density.

References

1. Shah A, Torres P, Tscharner R, Wyrsch N, Keppner H (1999) Science 285:692
2. Schropp REI, Carius R, Beaucarne G (2007) MRS Bull 32:219
3. van der Wilt P, Kane MG, Limanov AB, Firester AH, Goodman L, Lee J, Abelson J, Chitu AM, Im JS (2006) MRS Bull 31:461
4. Wang ZM, Jeurgens LPH, Wang JY, Mittemeijer EJ (2009) Adv Eng Mater 11:131
5. Wang ZM, Wang JY, Jeurgens LPH, Mittemeijer EJ (2008) Phys Rev Lett 100:125503
6. He D, Wang JY, Mittemeijer EJ (2005) Appl Phys A 80:501
7. Rosenberg R, Sullivan MJ, Howard JK (1978) In: Poate JM, Tu KN, Mayer JW (eds) Thin films-interdiffusion and reactions. Wiley, New York, p 13
8. Dutta I, Burkhard M, Kuwano S, Fujita T, Chen MW (2010) J Mater Sci 45:3367. doi:10.1007/s10853-010-4359-x
9. Koch CT, Sigle W, Höschen R, Rühle M, Essers E, Benner G, Matijevic M (2006) Microsc Microanal 12:506
10. Egerton RF (1996) Electron energy-loss spectroscopy in the electron microscope. Plenum Press, New York
11. Wang JY, Wang ZM, Mittemeijer EJ (2007) J Appl Phys 102:113523
12. Wang ZM, Wang JY, Jeurgens LPH, Mittemeijer EJ (2008) Phys Rev B 77:045424
13. Jeurgens LPH, Wang ZM, Mittemeijer EJ (2009) Int J Mater Res 100:1281
14. Massalski TB (1990) Binary alloy phase diagrams. ASM International, Materials Park